# Supporting Information for

# "Microscopic Study of Chain Deformation and Orientation in Uniaxially Strained Polymer Networks: NMR Results versus Different Network Models"

Maria Ott[*],[1] Roberto Pérez-Aparicio,[2] Horst Schneider,[1] Paul Sotta,[2] and Kay Saalwächter[*],[1]

[1]*Institut für Physik – NMR, Martin-Luther-Universität Halle-Wittenberg,
Betty-Heimann-Str. 7, 06120 Halle, Germany*

[2]*Laboratoire Polymères et Matériaux Avancés, CNRS/Rhodia-Solvay,
UMR 5268, 85 avenue des Frères Perret, F-69192 Saint Fons, France*

## SI1.   ^{1}H NMR SPECTROSCOPY

### A.   Basics

The determination of the distributions of the local residual dipolar coupling constants, $P(D_{res})$, was realized by a multiple-quantum (MQ) NMR experiment as described elsewhere [1, 2]. Basically, the NMR experiment provides two sets of data. Given the phase acquired under the DQ pulse sequence of duration $\tau_{DQ}$, $\phi_{DQ} = D_{res}P_2(\cos\theta)\tau_{DQ}$ ($\theta$ being the average segmental orientation), the build-up of the DQ intensity $I_{DQ}(\tau_{DQ}) = \langle\sin^2\phi_{DQ}\rangle_\theta R(2\tau_{DQ})$ mainly reflects DQ coherences that are dominated by intrachain spin-pair dipole-dipole couplings, and the reference intensity $I_{ref}(\tau_{DQ}) = \langle\cos^2\phi_{DQ}\rangle_\theta R(2\tau_{DQ}) + I_{tail}(\tau_{DQ})$ includes all signal which has not evolved into DQ coherences after a certain evolution time $\tau_{DQ}$ (Fig. SI 1).

Consequently, the sum $I_{sum} = I_{DQ} + I_{ref}$ contains the full dipolar refocused intensities and can serve as a norm, which decays only due to molecular motions occurring on the timescale of the experiment, as described by a transverse relaxation function
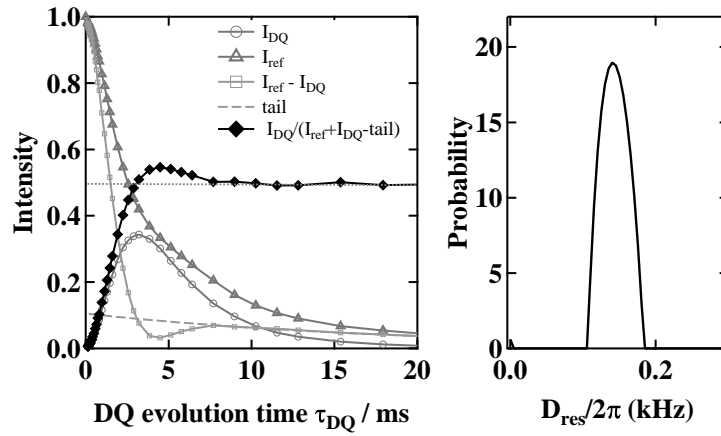


Figure SI 1: An MQ experiment provides two intensity functions that relax for long evolution times $\tau_{DQ}$: $I_{DQ}$ (circles) and $I_{ref}$ (triangles), as demonstrated for the unstretched sample NR1B in the left panel. The difference intensity $I_{ref} - I_{DQ}$ (squares) allows to reliably determine a tail function (dashed line) with an amplitude corresponding to the defect volume fraction of the sample. The overall intensity decay due to intermediate-timescale motions of the matrix can be removed by dividing $I_{DQ}$ by the term $I_{DQ} + I_{ref} - I_{tail}$ for each $\tau_{DQ}$ (rhombi). The normalized DQ intensity $I_{nDQ}$ enables the determination of residual dipole-dipole coupling distributions by Tikhonov regularization (right panel).

[*] Corresponding Authors:
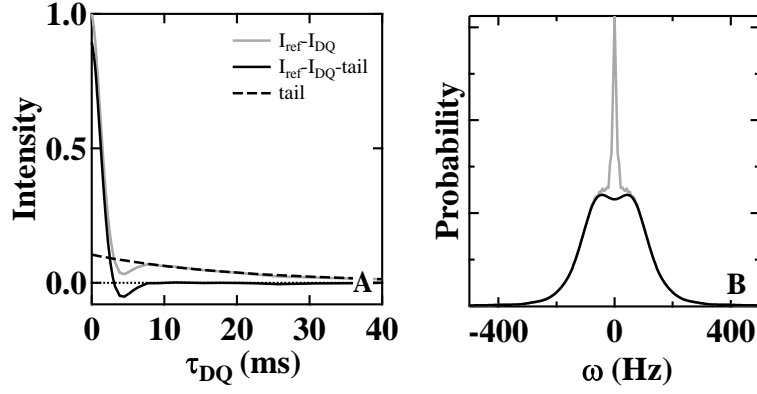maria.ott@physik.uni-halle.de
kay.saalwaechter@physik.uni-halle.de

**F**igure SI 2: $I_{\text{diff}}$ (grey line, left) and $I_{\text{diff}} - I_{\text{tail}}$ (black line, left), taken from Fig. SI 1, can be used to calculate dipolar spectra (right) using eq. SI2. The elastic defect fraction contribution is related to $I_{\text{tail}}$ (dashed line, left) and appears in the spectra as an additional zero frequency peak (right). The average dipolar interaction $D_{\text{res}}$ can be determined in a model-free way from the second moment of the spectra.

$R(2\tau_{\text{DQ}})$. While these relaxation processes are present in both intensities and can be removed by a point-by-point normalization, contributions of non-network components (generally) do not contribute to $I_{\text{DQ}}$ but lead to a slowly relaxing tail contribution to $I_{\text{ref}}$. Exploiting the 50-50 distribution of the signal among $I_{\text{DQ}}$ and the proper reference for network-only components beyond the maximum of the build-up curve, the difference $I_{\text{diff}} = I_{\text{ref}} - I_{\text{DQ}}$ most clearly reveals the non-elastomeric content of the sample. The long-time tail of $I_{\text{diff}}(\tau_{\text{DQ}})$ is a slowly decaying function which can often be well approximated by a single-exponential decay with an amplitude referring to the volume fraction of the defects. A subtraction of the exponential tail from the sum intensity eliminates the defect contribution, and a normalized DQ intensity build-up curve $I_{\text{nDQ}}$ is obtained:

$$I_{\text{nDQ}}(\tau_{\text{DQ}}) = \frac{I_{\text{DQ}}(\tau_{\text{DQ}})}{I_{\text{DQ}}(\tau_{\text{DQ}}) + I_{\text{ref}}(\tau_{\text{DQ}}) - I_{\text{tail}}(\tau_{\text{DQ}})} \ . \tag{SI1}$$

Such data taken on powder samples can now be subjected to a numerical distribution analysis of $D_{\text{res}}$ based upon Tikhonov regularization, as explained in the main text.

### B. Initial-rise analysis, moments and spectra

As a model-free alternative to the numerical distribution analysis, time-domain data equivalent to a Hahn-echo (pure dipolar dephasing) experiment can be calculated from the MQ data [3] using the phase relation $\phi_{\text{echo}} = \frac{3}{2}\phi_{\text{DQ}}$ [1], which amounts to a scaling of the time axis, and known trigonometric relations:

$$\begin{aligned} \widehat{I}_{\text{echo}}(t) &= \langle \cos\phi_{\text{echo}}\rangle \\ &= \left\langle \cos^2\left(2\frac{3}{2}\phi_{\text{DQ}}\right)\right\rangle - \left\langle \sin^2\left(2\frac{3}{2}\phi_{\text{DQ}}\right)\right\rangle \\ &\sim I_{\text{ref}} - I_{\text{DQ}}\left(-I_{\text{tail}}\right) \end{aligned} \tag{SI2}$$

With $\widehat{I}_{\text{echo}}(t) \sim I_{\text{diff}}$, a dipolar spectrum can be obtained by Fourier transformation. Such analyses of $I_{\text{diff}}$ are not only possible for an unstretched powder sample, but also for a selected sample orientation of a stretched sample or for the "artificial" powder average constructed from it, in the same way as for $I_{\text{nDQ}}$ (see eq. SI2). The difference between $I_{\text{diff}}$ and $I_{\text{nDQ}}$ is that the former is not corrected for incoherent relaxation (long-time decay), which means that the spectra still contain some (though weak) homogeneous line broadening.

As expected, the resulting dipolar spectra (Fig. SI 2) show a central peak only in case the non-elastic network contributions ($I_{\text{tail}}$) are not subtracted. The central peak can be directly related to compounds with zero residual dipolar interaction, e.g. defect chains or low-molecular impurities. The subtraction of the tail eliminates this contribution and leads to Gaussian-shaped spectra with an additional weak doublet. In stretched samples, the splitting includes contributions from partially oriented defect chains [4], while in unstretched samples (as shown in Fig. SI 2) it is also present and arises from multispin interactions. The latter
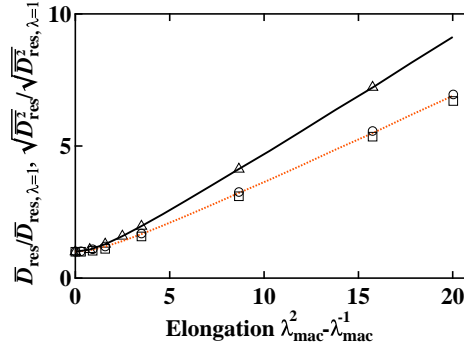
**F**igure SI 3: Comparison of theoretical predictions (homogeneous network, affine model) for the second and fourth moments of the extension ratio ($r = R(\lambda_{mac})/R_0$), $\langle r^2(\lambda_{mac}) \rangle$ and $\langle r^4(\lambda_{mac}) \rangle^{1/2}$ shown as dotted orange and solid black lines, respectively, with results based upon $D_{res} \sim r^2$ obtained from MQ NMR meta-data. $\overline{D}_{res}$ obtained from the Tikhonov regularization result (squares) and the half-sided average of the dipolar spectra (circles) agree with the former, while the second moment calculated from dipolar spectra agrees with the latter.

phenomenon is specific to spin dynamics among different quantum orders under the DQ pulse sequence [5] and is not apparent in a standard Hahn-echo experiment.

Average values $\overline{D}_{res}$ or $\sqrt{\overline{D_{res}^2}}$ can now be obtained in different ways, and a comparison of their ratio to the unstretched reference can be used as a consistency check (see Fig. 4C of the main paper). The first moment (arithmetic average) can either be obtained from the actual $D_{res}$ distribution obtained by regularization analysis, or from a half-sided integration of the dipolar spectra:

$$\overline{D}_{res} \sim \int_0^\infty \omega\, g(\omega)\, d\omega \bigg/ \int_0^\infty g(\omega)\, d\omega, \tag{SI3}$$

This procedure is only exact for vanishing homogeneous broadening (which "smears" data for $\omega < 0$ into the first quadrant), nevertheless, the data in Fig. 4C of the main paper proves the procedure to be robust for the case of MQ NMR data (we do not advise to do this for $^2$H spectra, where the homogeneous contribution is not known *a priori*).

The second moment used to calculate $\sqrt{\overline{D_{res}^2}}$ can also be obtained in various ways. Integration of dipolar spectra is an obvious one, as is its calculation from the known $D_{res}$ distribution. Alternatively, it can be obtained by fitting the initial rise of nDQ build-up curves, $I_{nDQ} \sim \overline{D_{res}^2} \tau_{DQ}^2$ to a parabola. Finally, time-domain data corresponding to dipolar spectra ($I_{diff}$) or the Fourier-transformed fit results to $^2$H spectra from the literature can be fitted to $\exp\{-k\overline{D_{res}^2}t^2\} \approx 1 - k\overline{D_{res}^2}t^2$. All these approaches yield largely equivalent results when applied to our data (see Fig. 4C of the main paper).

It is important to note that the theoretical description of the strain-dependent square-averaged $\sqrt{\overline{D_{res}^2}}(\lambda_{mac})$ is different from that of the first moment, eq. (16) of the main paper. A similar calculation for the average over all orientations $i$ yields

$$\frac{\sqrt{\overline{D_{res}^2}}(\lambda_{mac})}{\sqrt{\overline{D_{res,\lambda_{mac}=1}^2}}} = \frac{\sqrt{\langle R^4 \rangle_i}}{R_0^2} = \frac{1}{5}\left(\lambda_\parallel^4 + \frac{4\lambda_\parallel^2\lambda_\perp^2}{3} + \frac{8}{3}\lambda_\perp^4\right). \tag{SI4}$$

In order to demonstrate this difference and to analyze the consistency of the different moment determinations used to relate the experimental $D_{res}$ with the local deformation $r^2 = R^2/R_0^2$, we have generated $I_{nDQ}$ meta-data for the artificial powder average of the affine model (as explained in the next Section SI2), which leads to the widest $D_{res}$ distributions and the largest strain-dependent increase of its average among all models. The data in Fig. SI 3 demonstrate the difference between the relative first and second moments, and also shows that the different methods to extract the different averages of $D_{res}$ are quantitatively correct.

In contrast, our experimental data usually show $\overline{D_{res}^2} \approx \overline{D}_{res}^2$ within our accuracy limits (see Fig. 4C, main text). This is another demonstration of the deficiencies of the simple network models, and shows that only a full distribution analysis of $D_{res}$ rather than the study of just one type of moment enables a critical discussion. Only models that predict reasonably narrow distributions (leading to more similar first and second moments) are realistic ones.

## SI2.  NUMERICAL CALCULATIONS

### A.  General strategy

For the comparisons of the experimental results with theoretical predictions, we performed numerical calculations based upon a sufficiently large random set of isotropically distributed end-to-end vectors $R$. The apparent initial length distribution was chosen to be either represented by a $\delta$ function (representing the time average $R_0 = \langle R^2 \rangle^{1/2}$ over the usual instantaneous Gaussian $R$ distribution), or by alternative probability functions characterizing crosslinking inhomogeneities as taken from the experimental data. As described in the main text, these were for practical reasons implemented as additional length distributions of $R$, which mathematically corresponds to a simple convolution procedure.

The acquired phase in the DQ experiment is for a single residual coupling (a representative segment of a single type of sub-chain) written as $\phi_{DQ} = D_{res}P_2(\cos\theta)\tau_{DQ}$, where $\theta$ is its time-averaged orientation with respect to the magnetic field and $D_{res} \sim R^2/R_0^2$. Therefore, the DQ intensity of the entire system is proportional to the sum of the individual chains' contributions and reads:

$$I_{nDQ}(\tau_{DQ}) \sim \sum_i \sin^2\left(\frac{3D_{eff}}{5N}\frac{R_i^2}{R_0^2}P_2(\cos\theta_i)\tau_{DQ}\right). \tag{SI5}$$

Uniaxial stretching can be "simulated" by coordinate transformations of the differently oriented end-to-end vectors $R_i \to R'_i$, see Fig. 5 of the main text, using the characteristic ratios between the macroscopic and the local microscopic deformation, see eqs. (4–9) therein. The corresponding spectra were simply obtained as histograms in bins of fixed frequency width via the summation over all $i$ phases:

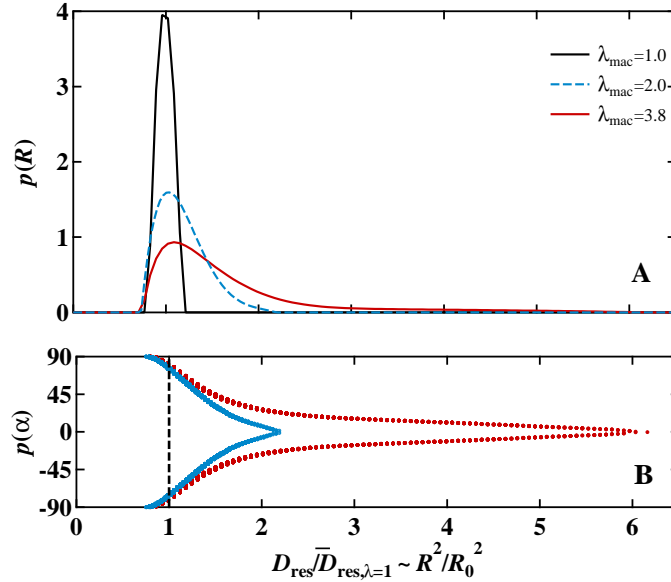$$\phi_{DQ}^i/\tau_{DQ} \sim \pm\frac{R_i^2}{R_0^2}P_2(\cos\theta_i). \tag{SI6}$$



Figure SI 4: A set of 10000 chains was generated, having the apparent $R$-distribution $p(R)$ as derived from the experiment (A) and an orientation distribution $p(\alpha)$ characterized by $\kappa$. The anisotropy paramter $\kappa$ was taken as a free variable to iteratively fit the simulated data to the anisotropic features of the experiments. The shown data sets correspond to the angle-dependent data shown in Fig. 10 of the main text.

## B. Anisotropy fit

The orientation dependence of the DQ intensity was fitted by using the random-set approach from above and an iterative refinement of the anisotropy parameter $\kappa$:

1. generation of a set of 10000 chains with an $R$ distribution, $p(R')$, corresponding to the length distribution of unixially deformed NR samples (SI Fig. 3A)

2. generation of an orientation distribution, $p(\alpha')$, by using $\tan\alpha'_i = \kappa\tan\alpha_i$ with an initial guess of $\kappa$ and an isotropic distribution $p(\alpha)$, where $\alpha$ describes the orientation of the chains with respect to the macroscopic elongation (see Fig. 5 of the main text) and $\kappa = \lambda^*_\perp/\lambda^*_\parallel$ with $\lambda^*_\perp$ and $\lambda^*_\parallel$ characterizing the orientational deformation ellipsoid as described in the main text. This approach can also be rationalized by defining new unit vectors, $\vec{e}_i = \{e_{\perp,i}, e_{\perp,i}, e_{\parallel,i}\}$, with:

$$e_{\perp,i} = \lambda^{*2}_{\perp,i}\sin^2\alpha_i / \left(\lambda^{*2}_{\parallel,i}\cos^2\alpha_i + \lambda^*_{\perp,i2}\sin^2\alpha_i\right) \tag{SI7}$$

$$= \kappa^2\sin^2\alpha_i / \left(\cos^2\alpha_i + \kappa^2\sin^2\alpha_i\right) \tag{SI8}$$

$$e_{\parallel,i} = \lambda^{*2}_{\parallel}\cos^2\alpha_i / \left(\lambda^{*2}_{\parallel,i}\cos^2\alpha_i + \lambda^{*2}_{\perp,i}\sin^2\alpha_i\right) \tag{SI9}$$

$$= \cos^2\alpha_i / \left(\cos^2\alpha_i + \kappa^2\sin^2\alpha_i\right) \tag{SI10}$$

3. it was assumed that longer chains appear at smaller angles and vice versa (SI Fig. 3B), imposing a correlation of the orientation with the value of $R$

4. the DQ intensities for a given evolution time $\tau_{DQ}$ were calculated using eq. SI3, normalized by the powder average and compared with the experimentally derived normalized intensity $I_{nDQ}/I^{pow}_{nDQ}$. $\tau_{DQ}$ was chosen such that $I_{nDQ}$ was approx. 0.1 ($\tau_{DQ}$ was 0.3 ms and 0.5 ms for the samples NR3X and NR1X, respectively)

5. $\kappa$ was iteratively adjusted to fit the experimental data sets (for results see Figs. 10 and 11 of the main text)

## SI3. LINESHAPE DECOMPOSITION OF $^2$H NMR SPECTRA

| Polymer | method | network type | defects | $M_c$ (g/mol) | Ref. |
|---|---|---|---|---|---|
| natural rubber | $^1$H MQ NMR | sulfur-vulcanized | 5% | 2100 | [4] |
| poly(dimethylsiloxane) | $^2$H NMR spectra | end-linked | 22% | 5000 (?) | [6] |
| poly($1,1,4,4-d_4$-butadiene) PB$_d-5-4$ | $^2$H NMR spectra | radically crosslinked | 30% | 19500 | [7] |
| PB$_d-3-5$ | $^2$H NMR spectra | radically crosslinked | 25% | 15900 | [7] |
| PB$_d-3-6$ | $^2$H NMR spectra | radically crosslinked | 32% | 11600 | [7] |
| PB$_d-Si-1$ | $^2$H NMR spectra | radically crosslinked , junction-labeled | 35% | 27000 | [7] |
| PB$_d-Si-3$ | $^2$H NMR spectra | radically crosslinked , junction-labeled | 28% | 15900 | [7] |
| poly($1,1,4,4-d_4$-butadiene) | $^2$H NMR spectra | peroxide-crosslinked | 22% | 6500 | [8] |
| poly(dimethylsiloxane) | $^2$H NMR spectra | end-linked | 38% | l0500 | [9] |

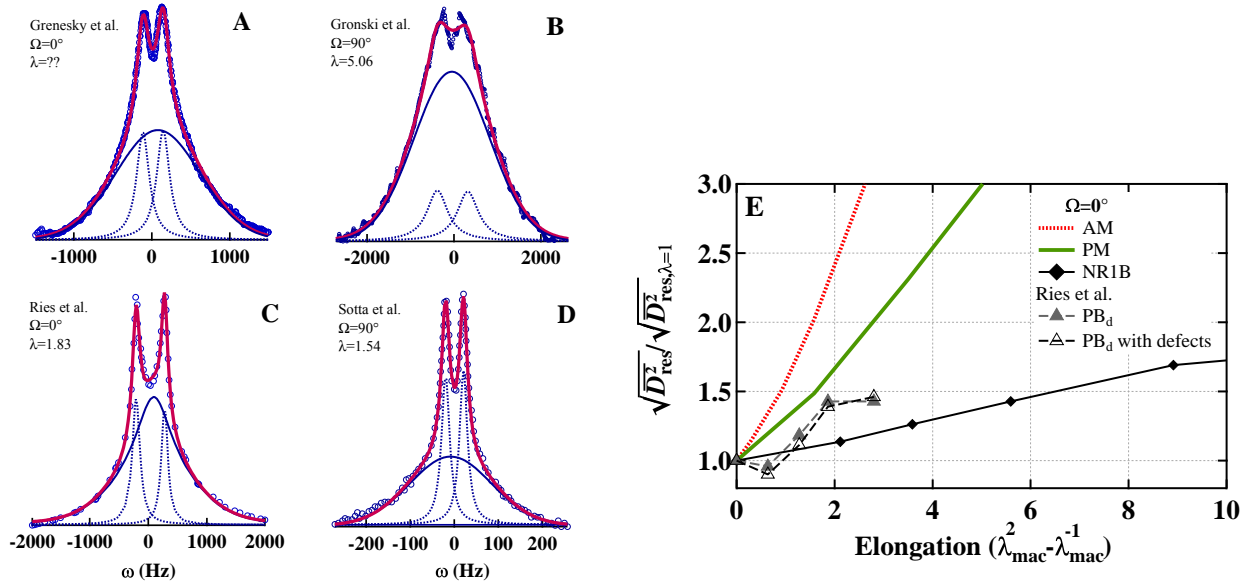SI Table I: Sample properties for Fig. 13 of the main text and Fig. SI 5.

**F**igure SI 5: Sample decompositions of $^2$H spectra from the literature. A: Genesky *et al.* [6], B: Gronski *et al.* [7], C: Ries *et al.* [8], D: Sotta *et al.* [9]. A pair of Lorentzians is attributed to the apparent defect contribution (splitting), which appears due to the orientating effect of the strained network matrix. The network response is described by a single Gaussian (A,B,D) or by the combination of a Gaussian and a Lorentzian (C). The right hand side (E) shows the comparison analogous to Fig. 13C,D of the main paper for the data of Ries *et al.*, which was obtained at a sample orientation of 0° (which means that the $^1$H MQ NMR data and the theoretical fits are different, as they depend on the orientation).

[1] K. Saalwächter. Proton multiple-quantum NMR for the study of chain dynamics and structural constraints in polymeric soft materials. *Progr. NMR Spectrosc.* **51** (2007) 1–35.

[2] W. Chassé, J. L. Valentín, G. D. Genesky, C. Cohen, and K. Saalwächter. Precise dipolar coupling constant distribution analysis in proton multiple-quantum NMR of elastomers. *J. Chem. Phys.* **134** (2011) 044907.

[3] K. Saalwächter and A. Heuer. Chain Dynamics in Elastomers as Investigated by Proton Multiple-Quantum NMR. *Macromolecules* **39** (2006) 3291–3303.

[4] R. Pérez-Aparicio, M. Schiewek, J. L. Valentín, H. Schneider, D. R. Long, M. Saphiannikova, P. Sotta, K. Saalwächter, and M. Ott. Local chain deformation and overstrain in reinforced elastomers: An nmr study. *Macromolecules* **46** (2013) 5549–5560.

[5] K. Saalwächter, P. Ziegler, O. Spyckerelle, B. Haidar, A. Vidal, and J.-U. Sommer. $^1$H multiple-quantum nuclear magnetic resonance investigations of molecular order distributions in poly(dimethylsiloxane) networks: Evidence for a linear mixing law in bimodal systems. *J. Chem. Phys.* **119** (2003) 3468–3482.

[6] G. D. Genesky, T. M. Duncan, and C. Cohen. Effect of Precursor Molar Mass on the 2H NMR Line Shapes of End-Linked PDMS Elastomers. *Macromolecules* **42** (2009) 8882–8888.

[7] W. Gronski, R. Stadler, and M. Maldaner Jacobi. Evidence of nonaffine and inhomogeneous deformation of network chains in strained rubber-elastic networks by deuterium magnetic resonance. *Macromolecules* **17** (1984) 741–748.

[8] M. E. Ries, M. G. Brereton, P. G. Klein, I. M. Ward, P. Ekanayake, H. Menge, and H. Schneider. Contributions to the Total Orientation of Deformed Elastomers Arising from the Network Structure and Chain Interactions As Measured by NMR. *Macromolecules* **32** (1999) 4961–4968.

[9] P. Sotta, J. Deloche, B.and Herz, A. Lapp, D. Durand, and J. C. Rabadeux. Evidence for short-range orientational couplings between chain segments in strained rubbers: a deuterium magnetic resonance investigation. *Macromolecules* **20** (1987) 2769–2774.